NASA Technical Memorandum 106757

Computational Analysis in Support of the SSTO Flowpath Test

Beverly S. Duncan
NYMA, Inc.
Engineering Services Division
Brook Park, Ohio

and

Charles J. Trefny
Lewis Research Center
National Aeronautics and Space Administration
Cleveland, Ohio

October 1994

National Aeronautics and Space Administration

Contents

List of Tables

List of Figures

1 Two-Dimensional Boundary Layer Analysis of CDE

1.1 Objective

The objective of this portion of the computational analysis is to obtain the boundary layer displacement and momentum thicknesses at the cowl lip station for the NASP Concept Demonstrator Engine (CDE) at the Mach 5, 6.28 and 6.80 conditions in the NASA Langley 8' High Temperature Tunnel (8' HTT). These values are to be compared to those calculated for the SSTO Flowpath Model as installed in the NASA Lewis 1 foot by 1-foot Supersonic Wind Tunnel (1x1 SWT) with various boundary layer diverter heights, to determine the diverter height which provides the best simulation at each Mach number.

1.2 Approach

The CDE model consists of an 8 degree wedge followed by seven 1/2 degree compressions. Table 1 gives the coordinates for this planar surface. A 100x65 point grid was generated for this surface using the grid generation package INGRID2D [2]. The grid was clustered toward the surface using a hyperbolic stretching function to give a $y^+ < 1$ for the first grid point off the wall at x = 97.43 inches. In addition, the grid was designed to be exactly normal to the surface so that integration of the profiles could be completed along a single grid line. See Figure 1 for a diagram of this grid. The outer boundary of the grid was located far enough away from the surface so that edge conditions could be well defined for all cases.

x (inches)	y (inches)	
0.000	0.000	model leading edge
41.122	5.779	
51.216	7.288	
60.413	8.745	
68.825	10.152	
76.549	11.514	
83.670	12.834	
90.258	14.115	
97.431	15.574	cowl lip station

Table 1: Coordinates for the CDE ramp.

The Navier-Stokes code PARC2D [1] was used to calculate the turbulent flow over the CDE ramp for the flow conditions given in Table 2. Although the Langley 8' HHT uses a methane combustion process to heat the air, the molecular weight and ratio of specific heats are close to those of air. Therefore, most of the calculations were performed using air properties. To assess the sensitivity of the results to a change in the ratio of specific heats, the Mach 6.28 case was also performed assuming a ratio of specific heats of 1.3. One calculation was also performed at Mach 6.28 with a cold wall, $T_{wall} = T_\infty = 399R$.

All the calculations were starting using a uniform inflow plane set to the freestream conditions given in Table 2. The outflow boundary and the far field boundary were extrapolated from the upstream flow conditions. A no-slip wall was imposed on the body surface.

The displacement and momentum thickness were determined using the compressible Von Karmen integral relations,

$$\delta^* = \int_0^\delta \left(1 - \frac{\rho\hat{U}}{\rho_e\hat{U}_e}\right) d\hat{y} \tag{1}$$

$$\Theta = \int_0^\delta \frac{\rho\hat{U}}{\rho_e\hat{U}_e}\left(1 - \frac{\hat{U}}{\hat{U}_e}\right) d\hat{y}. \tag{2}$$

where, $\hat{y}$ is the direction normal to the surface. Since the grid is orthogonal to the surface, the above integrations were performed along the normal grid line. The velocity, $\hat{U}$ is velocity parallel to the surface and is found from the simple geometric rotation, $\hat{U} = u\cos\alpha + v\sin\alpha$, where α is the body slope. The predicted values of δ^* and Θ at the cowl lip, $x_{body} = 97.43$ inches, are given in Table 3.

Figure 2 shows the axial distribution for momentum and displacement thickness as predicted by PARC2D at Mach 5. The dimensions for both momentum and displacement thickness are given in inches. The spikes in displacement thickness and to a lesser extent in momentum thickness result from the compression waves stemming from the $\frac{1}{2}$ degree compressions. Similar axial boundary layer property predictions are given in Figure 3 for Mach 6.28. As the Mach number is increased further, and the Reynolds number reduced, the boundary layer growth is more pronounced as can be seen in Figure 4.

At Mach 6.28, a cold wall ($T_{wall} = 399$ R) reduces the overall boundary layer growth. See Figure 3. The increase in density near the wall reduces the displacement thickness by approximately thirty percent at the last axial station. A reduction in the ratio of specific heats does not greatly effect the momentum thickness, as can be seen by comparing the curves in Figure 3. However, the displacement thickness is increased by approximately ten percent at the last x station.

1.3 Conclusions

As the Mach number is increased and the Reynolds number decreased, the boundary layer growth rate increases on the CDE ramp for an adiabatic wall. Cooling the wall reduces the displacement thickness but increases the momentum thickness because of the elevated density levels near the wall. A variation in the ratio of specific heats leaves the momentum thickness unchanged but slightly decreases the displacement thickness growth rate.

Mach	Re (ft^{-1})	γ	P_{static} (psia)	T_{static} (deg R)	wall cond.
5.00	1.758E06	1.4	.509	395.	adiabatic
6.28	1.211E06	1.4	.283	399.	adiabatic
6.28	1.211E06	1.4	.283	399.	$T_{wall} = 399R$
6.28	1.211E06	1.3	.283	399.	adiabatic
6.80	1.017E06	1.4	.243	431.	adiabatic

Table 2: Flow conditions in the NASA Langley 8' High Temperature Tunnel.

$Re(ft^{-1})$	Mach no.	δ^* (PARC)	Θ (PARC)	δ^* (STAN5)	Θ (STAN5)
1.758E6	5.00	0.3795 in.	0.0470 in.	0.3956 in.	0.0521 in.
1.211E6	6.28	0.4495 in.	0.0418 in.	0.4580 in.	0.0446 in.
1.211E6	6.28, $T_{wall} = 399R$	0.2858 in.	0.0550 in.	0.3112 in.	0.0574 in.
1.211E6	6.28,$\gamma = 1.3$	0.5008 in.	0.0502 in.	——	——
1.017E6	6.80	0.5194 in.	0.0436 in.	0.4852 in.	0.0431 in.

Table 3: Displacement and momentum thicknesses on the CDE ramp at x=97.43 inches.

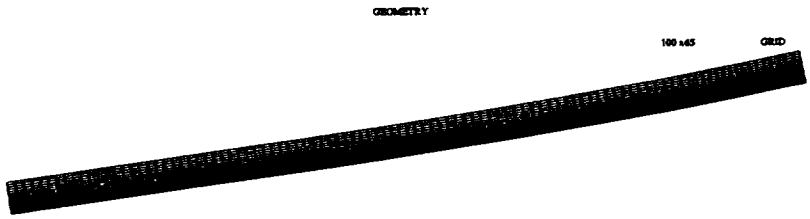

Figure 1: Grid distribution used for CDE ramp analysis.

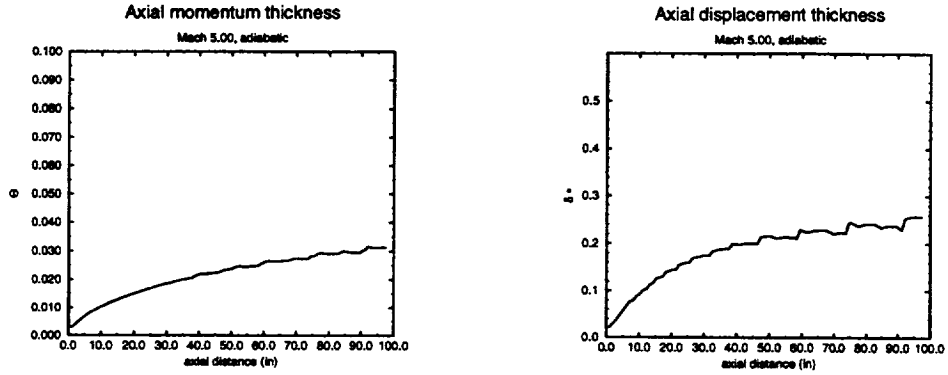

Figure 2: Axial momentum and displacement thicknesses at Mach 5.0 with adiabatic walls.

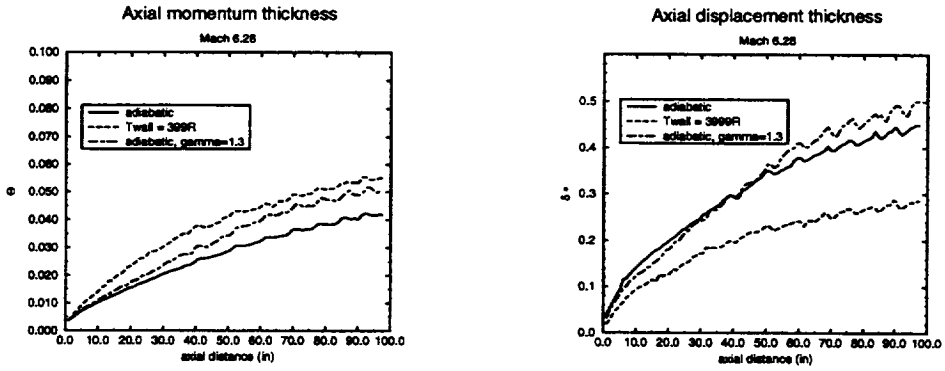

Figure 3: Axial momentum and displacement thicknesses at Mach 6.28.

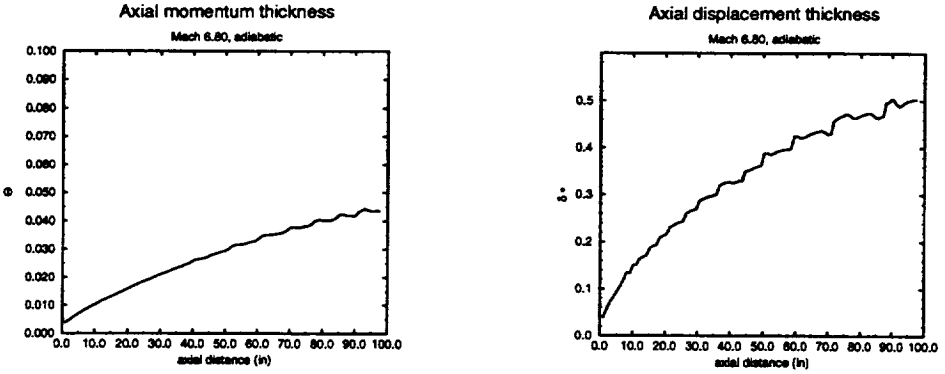

Figure 4: Axial momentum and displacement thicknesses at Mach 6.8 with adiabatic walls.

2 Two-Dimensional Analysis for the SSTO Flowpath Model

2.1 Objective

The objective of this study was to determine the diverter heights in the NASA Lewis 1x1 Supersonic Wind Tunnel which would best reproduce the boundary layer profiles found for the larger CDE model tested in the NASA Langley 8' High Temperature Tunnel. To achieve this, the momentum and displacement thicknesses were determined for the Mach 4, 5 and 5.5 conditions for several facility boundary layer diverter heights. These boundary layer values were plotted against those computed in the previous section for the CDE model.

2.2 Approach

The incoming facility boundary layer was described using experimental pitot pressure measurements obtained for the four nozzles. Since these profiles had been obtained at different flow conditions, it was necessary to rescale them before they could be applied to the current study. This static pressure required to rescale the pitot pressure profile was determined based on the freestream Mach number in the tunnel. Assuming that this deduced freestream static pressure remained constant through the boundary layer, a Mach number profile was obtained. The resulting nondimensional pitot pressure profiles and the Mach number profiles are shown in Figures 5, 6, 7, and 8. Using these Mach number profiles and assuming that the flow was adiabatic, $H_{wall} = H_{\infty}$, the incoming velocity and thermal boundary layers were determined. Five diverter heights were simulated by shifting the y coordinate in these profiles by 0.0, 0.25, 0.5, 1.0 or 1.5 inches. This adjusted Mach number profile was then used as the inflow plane to PARC2D.

The SSTO Flowpath Model is a 0.3 scale version of the CDE ramp, given in the previous section, which has been rotated by nine degrees and the initial 60.413 inches has been eliminated. This set of x-y coordinates are given in Table 4. For this shortened model, the grid size was reduced to 40x65. The grid generation was performed exactly as described for the CDE calculations and will not be readdressed; except to say that the y^+ at the last axial station was less than one when there was no incoming boundary layer. This grid dicretization should adequately resolve the boundary layer for all diverter heights.

PARC2D was again used to calculate the turbulent, adiabatic flow over the SSTO Flowpath Model ramp. The predicted displacement and momentum thicknesses are given in Tables 6 and 7 for four Mach numbers and five diverter heights. The displacement and momentum thicknesses listed for the CDE ramp are for the adiabatic wall cases and have been rescaled to match the SSTO scale.

At diverter heights less than 0.5 inches, the boundary layer is dominated by the ingested facility shear layer. The resulting momentum and displacement thicknesses at x=11.3 inches are significantly greater than the boundary layer produced on the CDE model at the corresponding station. A diverter height of 1.5 places the model outside the facility shear layer and the predicted momentum and displacement thicknesses are lower than produced on the CDE model. A boundary layer diverter height of 1 inch produces the best simulation for the boundary layer development on the CDE ramp. This result is consistent for all three Mach numbers compared.

Figures 13 through 15 compared the Mach number and pitot pressure profiles between the CDE model and the SSTO model assuming a 1 inch diverter height. (Since the NASA Langley High Temperature Wind Tunnel cannot run at conditions which would correspond to the Lewis Supersonic Wind Tunnel conditions at Mach 3, this portion of the study has not been performed for this Mach number.) These profiles are at the last computed station which is a plane normal to the ramp at the cowl lip leading edge. As can be seen, the overall boundary layer thickness is compatible between the two flow situations. However, the more diffuse nature of the ingested facility boundary layer used in the SSTO predictions caused a more rounded boundary layer edge.

2.3 Conclusions

Two-dimensional calculations were performed on the initial ramp section of SSTO flowpath model. The boundary layer properties predicted for five facility boundary layer diverter heights were compared to the boundary layer properties predicted for the CDE ramp model. From this comparison, a 1" diverter height was determined to give the best simulation of the boundary layer growth from the longer CDE model.

x (inches)	y (inches)
0.000	0.000
2.558	0.022
4.911	0.063
7.083	0.120
9.095	0.190
11.289	0.287

Table 4: Coordinates for the SSTO Flowpath Model.

Mach	Re (ft^{-1})	P_{static} (psia)	T_{static} (deg R)	wall cond.
2.90	6.2047E6	1.0889	194.	adiabatic
3.93	1.627E07	1.0867	123.	adiabatic
4.88	8.405E06	0.3118	99.2	adiabatic
5.55	6.568E06	0.1774	86.9	adiabatic

Table 5: Flow conditions in the NASA Lewis 1'x'1' Supersonic Wind Tunnel.

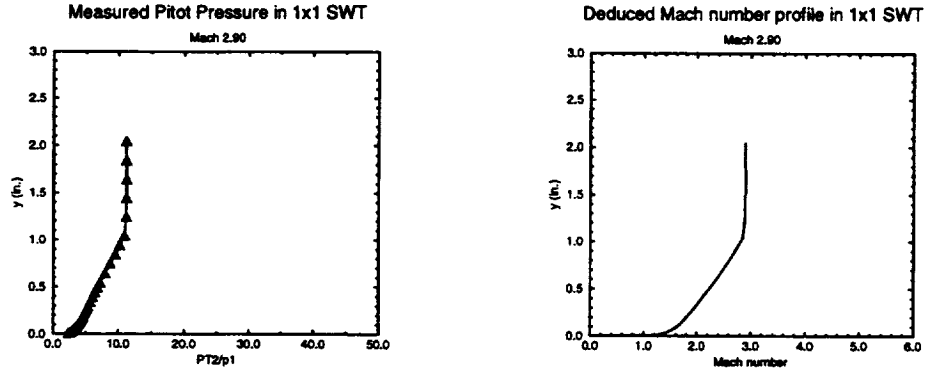

Figure 5: Pitot pressure and Mach number profiles for the NASA Lewis 1x1 Supersonic Wind Tunnel with the Mach 3.0 nozzle.

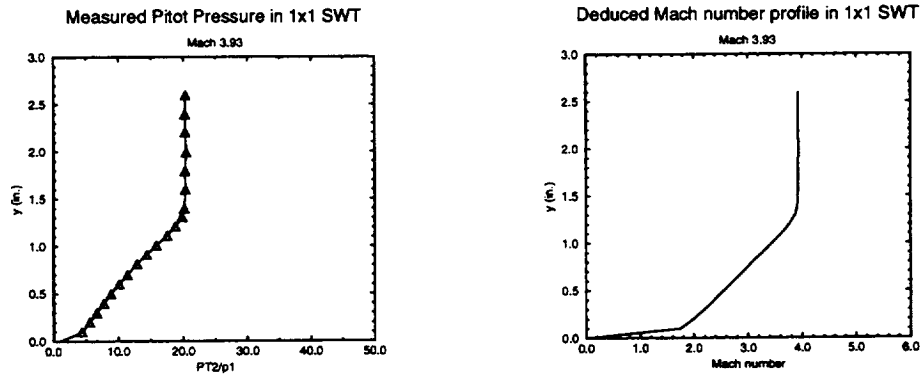

Figure 6: Pitot pressure and Mach number profiles for the NASA Lewis 1x1 Supersonic Wind Tunnel with the Mach 4.0 nozzle.

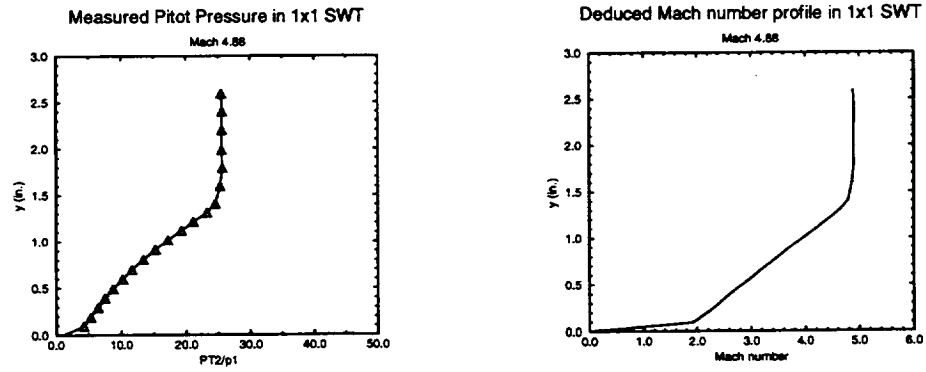

Figure 7: Pitot pressure and Mach number profiles for the NASA Lewis 1x1 Supersonic Wind Tunnel with the Mach 5.0 nozzle.

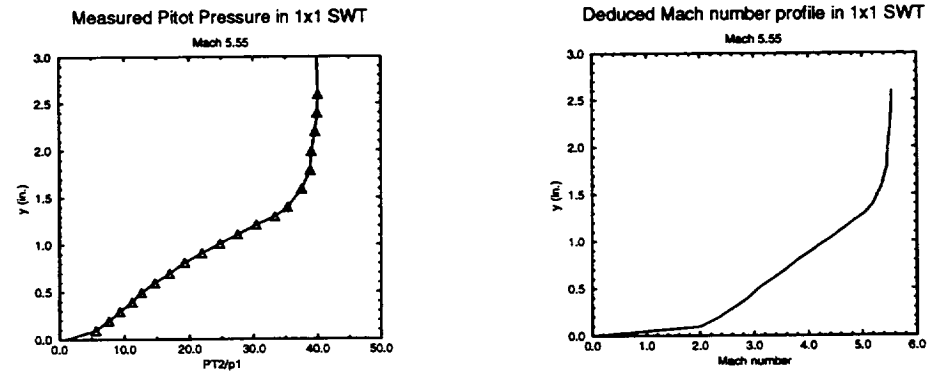

Figure 8: Pitot pressure and Mach number profiles for the NASA Lewis 1x1 Supersonic Wind Tunnel with the Mach 5.5 nozzle.

$Re(ft^1)$	Mach no.	δ^*_{SSTO},0.0 inches	δ^*_{SSTO},0.25 inches	δ^*_{SSTO},0.50 inches	δ^*_{SSTO},1.00 inches	δ^*_{SSTO}, 1.5 inches	δ^*_{CDE} (rescaled)
2.068E6	2.90	0.33406	0.21342	0.12299	0.04887	0.04573	——
1.626E7	3.93	0.49180	0.32170	0.20773	0.05946	0.02716	0.11385
8.405E6	4.88	0.56947	0.42501	0.30467	0.12584	0.08315	0.13486
6.568E6	5.55	0.58756	0.46243	0.32614	0.15100	0.09995	0.15583

Table 6: Displacement thickness on the Lewis model ramp at x=11.3 inches.

$Re(ft^1)$	Mach no.	Θ_{SSTO},0.0 inches	Θ_{SSTO},0.25 inches	Θ_{SSTO},0.50 inches	Θ_{SSTO},1.00 inches	Θ_{SSTO}, 1.5 inches	Θ_{CDE} (rescaled)
2.068E6	2.90	0.07763	0.05225	0.02994	0.01081	0.00964	——
1.627E7	3.93	0.07113	0.05232	0.03457	0.00899	0.00376	0.01410
8.405E6	4.88	0.06150	0.04943	0.03484	0.01336	0.00783	0.01254
6.568E6	5.55	0.05752	0.04538	0.03375	0.01509	0.00854	0.01308

Table 7: Momentum thickness on the Lewis model ramp at x=11.3 inches.

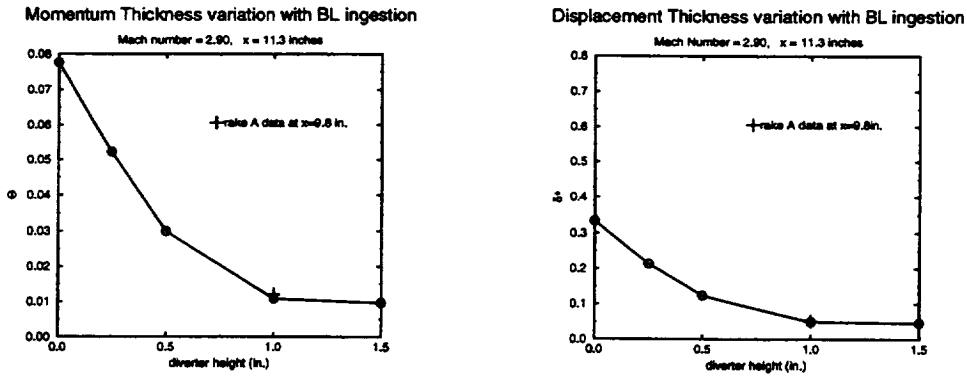

Figure 9: Momentum and displacement thicknesses at Mach 2.90 with adiabatic walls.

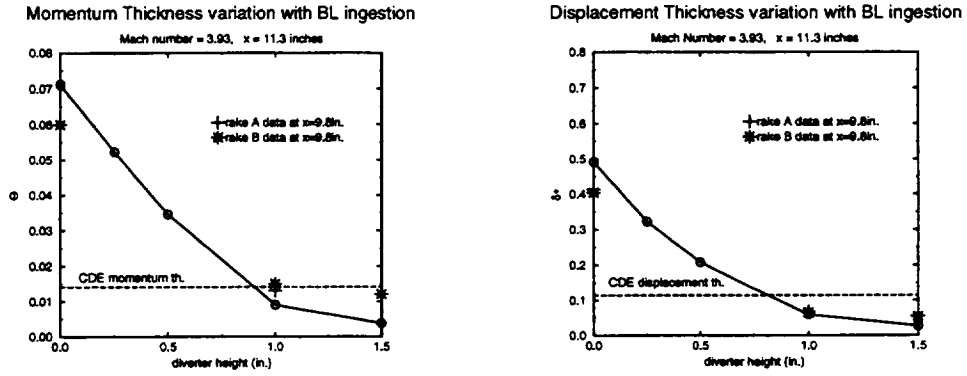

Figure 10: Momentum and displacement thicknesses at Mach 3.93 with adiabatic walls.

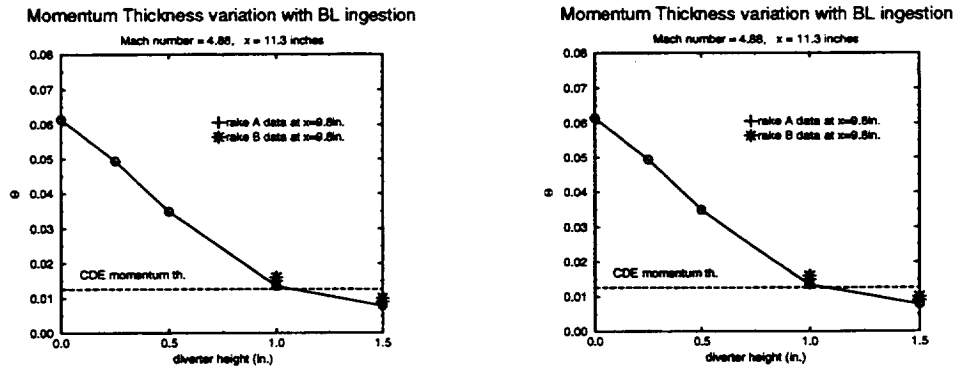

Figure 11: Momentum and displacement thicknesses at Mach 4.88 with adiabatic walls.

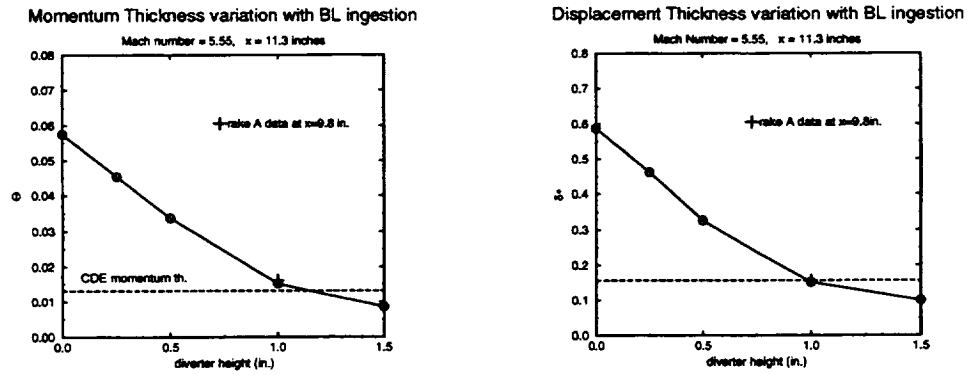

Figure 12: Momentum and displacement thicknesses at Mach 5.55 with adiabatic walls.

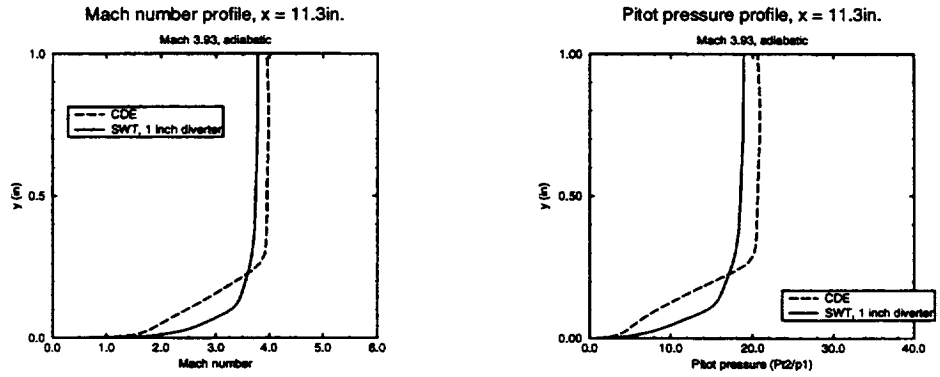

Figure 13: Mach number and pitot pressure profile comparison at the cowl lip stations between the CDE predictions and the SSTO predictions with a 1 inch diverter height at Mach 3.93.

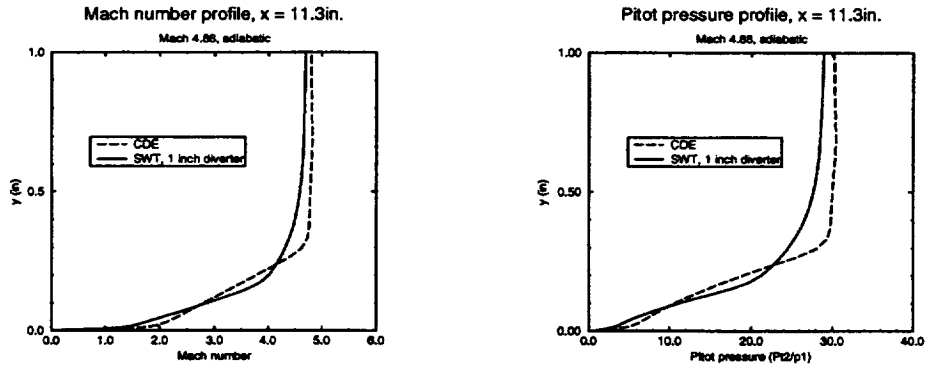

Figure 14: Mach number and pitot pressure profile comparison at the cowl lip stations between the CDE predictions and the SSTO predictions with a 1 inch diverter height at Mach 4.88.

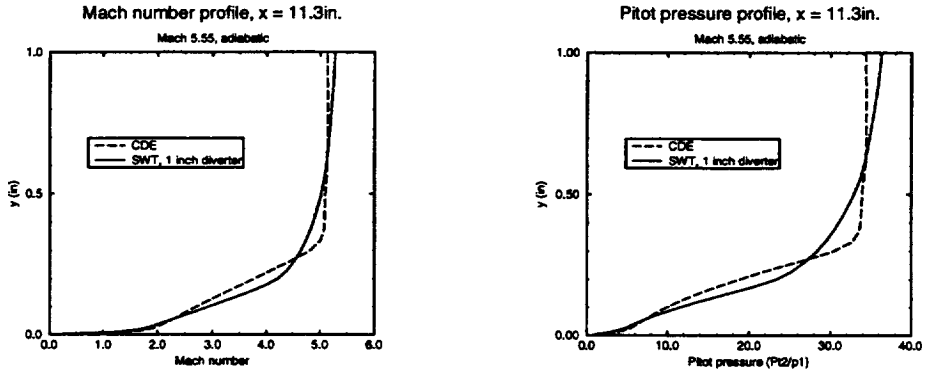

Figure 15: Mach number and pitot pressure profile comparison at the cowl lip stations between the CDE predictions and the SSTO predictions with a 1 inch diverter height at Mach 5.55.

3 CFD Compared to Measured Boundary Layer Profiles

3.1 Objective

The boundary layers for all five Mach numbers and with four facility boundary layer diverter heights were calculated using the two-dimensional version of PARC. This information was compared to the available experimental data. Profiles were also calculated for several cases in the test matrix where the lip rakes had been removed. Additionally, the computational results will be used to provide static profile information at the lip rake station.

3.2 Approach

The two-dimensional calculations documented in the previous section were compared to the available experimental data[3]. Two rakes were placed at x=9.8 inches from the SSTO leading edge. The "B" rake was placed on the model centerline and the "A" rake was outboard of the centerline at z=1.682 toward the splitter sidewall. Upstream of the cowl lip, the model should be essentially two-dimensional so that the "A" and "B" rake should be identical. However, there appears to be some small three-dimensional influences measured by the "A" rake which are more pronounced at the lowest Mach number.

Since the model has been placed in the tunnel using an aircraft orientation, the normal distance is given as increasing in the negative direction. For the computations, the grid is perfectly orthogonal so the profiles are taken along the grid line at x=9.8 inches from the leading edge of the ramp. Figures 16 and 17 indicate that the ramp boundary layer is dominated by the incoming facility boundary layer. The thick, near wall viscous flow gives the pitot pressure and Mach number profiles a rounded edge. At a diverter height of one inch, in Figure 18 most of the facility boundary layer has been diverted and the boundary layer edge is more definitive. The computations compare very well with the experimental data obtained for this flow condition. At this lower Mach number, the compression waves stemming from the 1/2 degree compressions are weakest and the inviscid portion of the profiles have a less "wavy" appearance than will be seen at the higher Mach numbers. When the diverter height is at its highest setting the viscous region is much smaller and the boundary layer edge is clearly defined, as can be seen in Figure 19.

In Figure 20 the pitot pressure normalized by the freestream total pressure is compared to the experimental data. The slope of the predicted pitot pressure above y=-1.4 inches matches the experimental measurement, however the computations predict a thicker boundary layer. For a Mach number of 3.93, both the experimental data and the computations are in agreement for the inviscid portion of the profile. The static pressure ratio shows the effect of the series of 1/2 degree compressions along the ramp surface. Figure 21 gives the predicted profiles for Mach 3.93 with the diverter height set to 0.5 inches. There is no data for comparison at this condition. At Mach 3.93 with a 1.0 inch diverter height the predicted pitot pressure compares very well to the "B" rake; see Figure 22. As previously noted, the "A" rake appears to be picking up some three-dimensional influences. With the diverter height set to 1.5 inches no facility boundary layer is ingested into the flowfield. For this condition, there is a discrepancy between the predicted and measured pitot pressures as can be seen in Figure 23. The computations predict a sharp boundary layer edge at approximately y=-0.09 inches above the ramp. However, the measured pitot pressure indicate a thicker boundary layer thickness and a more rounded profile. Whether this could be the result of the rake disturbing the boundary layer is uncertain.

At Mach 3.93 the wall static pressure can be assumed to be independent of the diverter height. As the diverter height is varied, the static pressure ratio at the wall increases only marginally from $\frac{p_w}{p_\infty} = 1.24$ at 0.0 inches to $\frac{p_w}{p_\infty} = 1.29$ at 1.5 inches.

Figures 24 and 25 show the predicted profiles for Mach 4.88 with diverter heights of 0.0 and 0.5 inches respectively. Unfortunately, there is no data for these conditions. With a diverter height of 1.0 inch, the measured normalized pitot pressure compares very well to the predicted values; see Figure 26. At this Mach number, the "A" rake is nearly coincident with the "B" rake indicating that any three-dimensional effects are minimal. Near the boundary layer edge, there is some discrepancy between the data and the computations. In this region the data indicates a larger normalized pitot pressure overshoot. However, above and below this region the two are in good agreement. When the facility boundary layer diverter height is set to 1.5 inches the inviscid portion of the flow shown in Figure 27 is again in very good agreement but with the measurements indicating a thicker boundary layer.

As the diverter height is increased for the Mach 4.88 condition, the static pressure ratio at the wall increases

from $\frac{p_w}{p_\infty} = 1.28$ at 0.0 inches to $\frac{p_w}{p_\infty} = 1.38$ at 1.5 inches.

The computed profiles for the Mach 5.6 test condition for all diverter heights are given in Figures 28 through 31. At this Mach number, only one set of experimental measurements were taken at a diverter height of 1.0 inch using the "A" rake. Looking in detail at this case, given in Figure 30, the data again has a more pronounced normalized pitot pressure overshoot than predicted by the computations. In the near wall region, the measurements and the calculations are in agreement. Likewise, in the inviscid region the data and the calculations agree. The reason for this discrepancy is unclear. This discrepancy may be more three-dimensional effects influencing the "A" rake.

The wall static pressure is very dependent upon the facility boundary layer diverter height for the Mach 5.55 flow condition. Since this is the lowest Reynolds number case, the thick incoming facility boundary layer with a 0.0 inch diverter height acts as a buffer to the series of compression waves from the 1/2 degree turning angles. In Figure 28, the static pressure ratio increases almost smoothly from its freestream value to $\frac{p_w}{p_\infty} = 1.31$ at the wall. With the diverter height set to 1.5 inches, the series of compressions are noticeable through the static pressure profile where the pressure ratio increases from its freestream value to $\frac{p_w}{p_\infty} = 1.45$ at the wall.

The momentum and displacement thicknesses near the rake station, x=9.8 inches, are given in Tables 8 and 9. This axial station is just past the last 1/2 degree turning angle or approximately 1.5 inches upstream of the cowl lip. Generally, the displacement thickness at x=9.8 is less than reported in Table 6 at the cowl lip station.

3.3 Conclusions

The computed pitot pressure profiles at the rake station were compared to the available experimental data. In general, the comparison showed very consistent profiles between the data and the computations. When the full facility boundary layer was ingested, the experimental data indicated a thinner boundary layer, but the overall profile shape was comparable. For the cases where the facility boundary layer was not ingested, diverter heights of 1.5 inches, the data indicated a softer boundary layer edge than the computations.

$Re(ft^1)$	Mach no.	δ^*_{SSTO},0.0 in.	δ^*_{SSTO},0.50 in.	δ^*_{SSTO},1.00 in.	δ^*_{SSTO}, 1.5 in.	
6.205E6	2.90	0.3399	0.1228	0.0438	0.0424	CFD
6.205E6	2.90	—	—	0.051	—	data, rake A
1.626E7	3.93	0.4902	0.2091	0.0549	0.0273	CFD
1.626E7	3.93	0.413	—	0.068	0.056	data, rake A
1.626E7	3.93	0.404	—	0.065	0.054	data, rake B
8.405E6	4.88	0.5734	0.3003	0.1236	0.0755	CFD
8.405E6	4.88	—	—	0.132	0.059	data, rake A
8.405E6	4.88	—	—	0.132	0.074	data, rake B
6.568E6	5.55	0.6111	0.3258	0.1070	0.0902	CFD
6.568E6	5.55	—	—	0.155	—	data, rake A

Table 8: Displacement thickness on the Lewis model ramp at x=9.8 inches.

$Re(ft^1)$	Mach no.	Θ_{SSTO},0.0 in.	Θ_{SSTO},0.50 in.	Θ_{SSTO},1.00 in.	Θ_{SSTO}, 1.5 in.	
6.205E6	2.90	0.0770	0.0296	0.0099	0.0090	CFD
6.205E6	2.90	—	—	0.012	—	data,rake A
1.627E7	3.93	0.0715	0.0346	0.0133	0.0038	CFD
1.627E7	3.93	0.060	—	0.013	0.012	data, rake A
1.627E7	3.93	0.060	—	0.015	0.012	data, rake B
8.405E6	4.88	0.0617	0.0329	0.0100	0.0073	CFD
8.405E6	4.88	—	—	0.015	0.009	data, rake A
8.405E6	4.88	—	—	0.016	0.010	data, rake B
6.568E6	5.55	0.0522	0.0299	0.0104	0.0077	CFD
6.568E6	5.55	—	—	0.016	—	data, rake A

Table 9: Momentum thickness on the Lewis model ramp at x=9.8 inches.

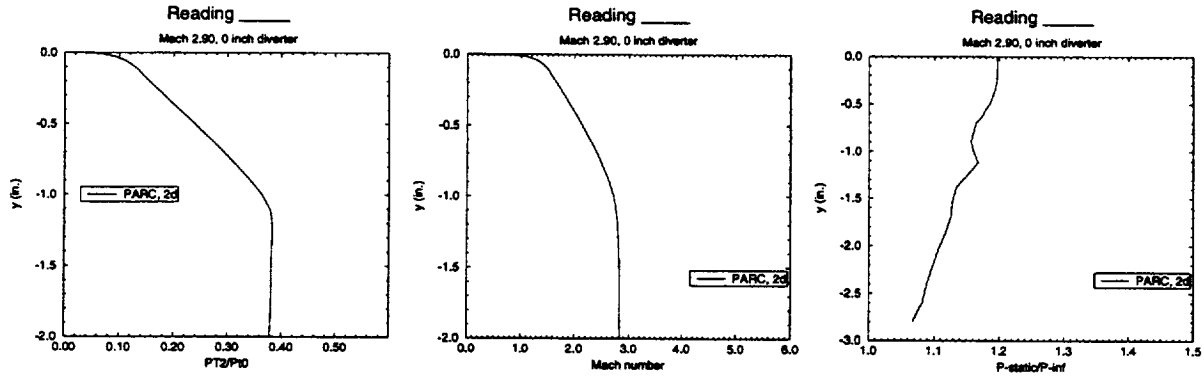

Figure 16: Boundary layer profiles for Mach 2.90 with a 0.0 inch diverter height.

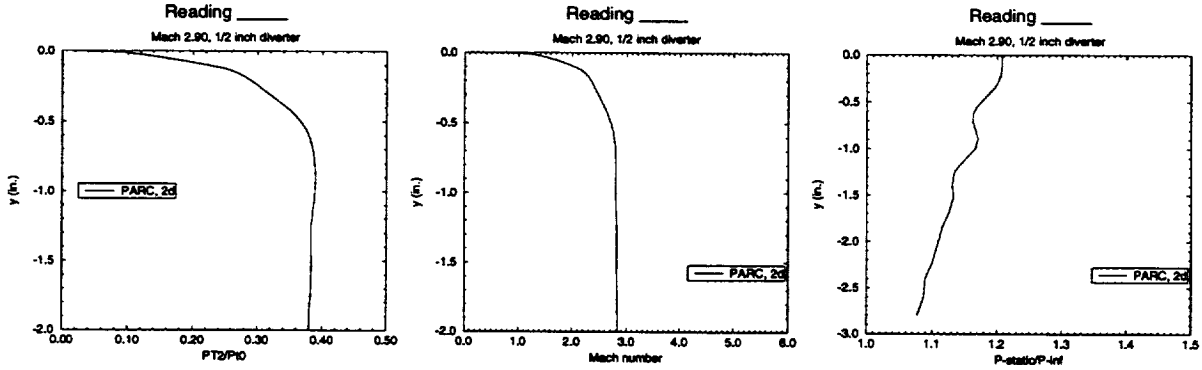

Figure 17: Boundary layer profiles for Mach 2.90 with a 0.5 inch diverter height.

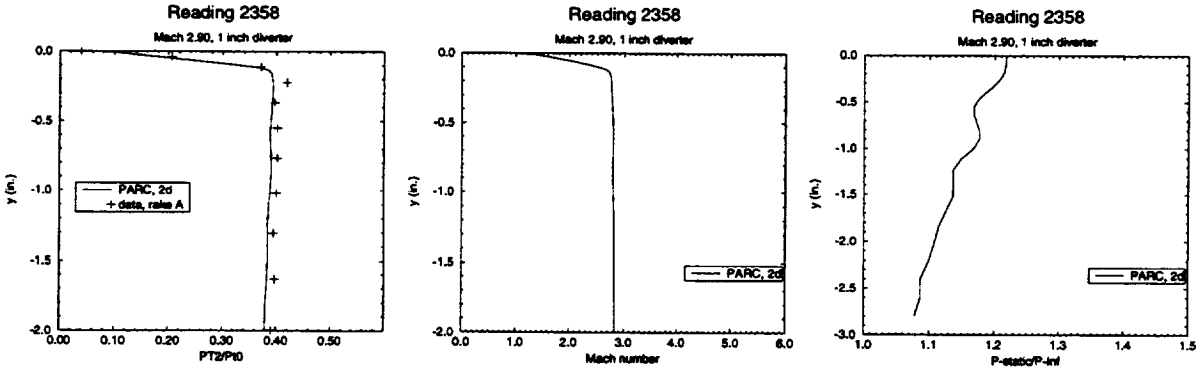

Figure 18: Boundary layer profiles for Mach 2.90 with a 1.0 inch diverter height.

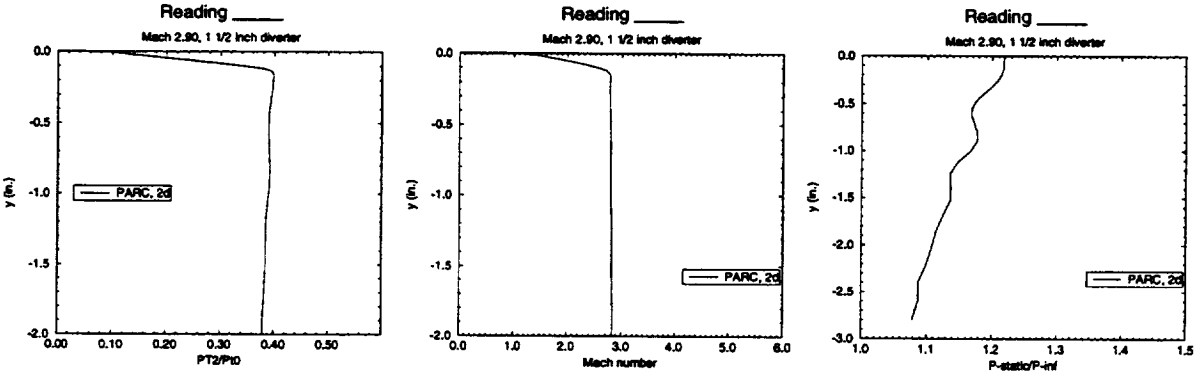

Figure 19: Boundary layer profiles for Mach 2.90 with a 1.5 inch diverter height.

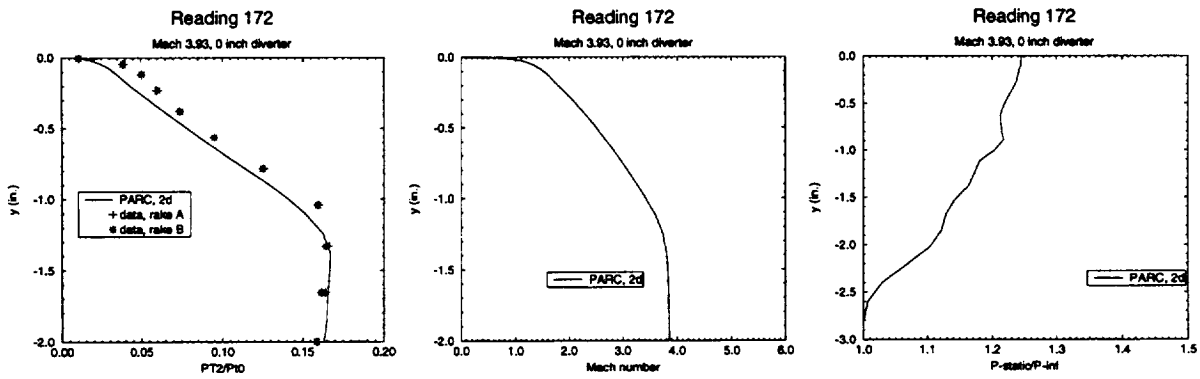

Figure 20: Boundary layer profiles for Mach 3.93 with 0.0 inch diverter height.

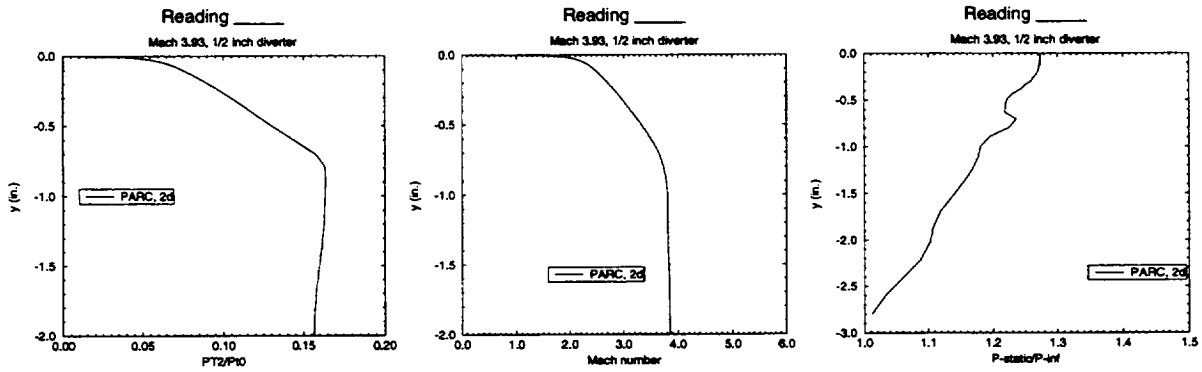

Figure 21: Boundary layer profiles for Mach 3.93 with 0.5 inch diverter height.

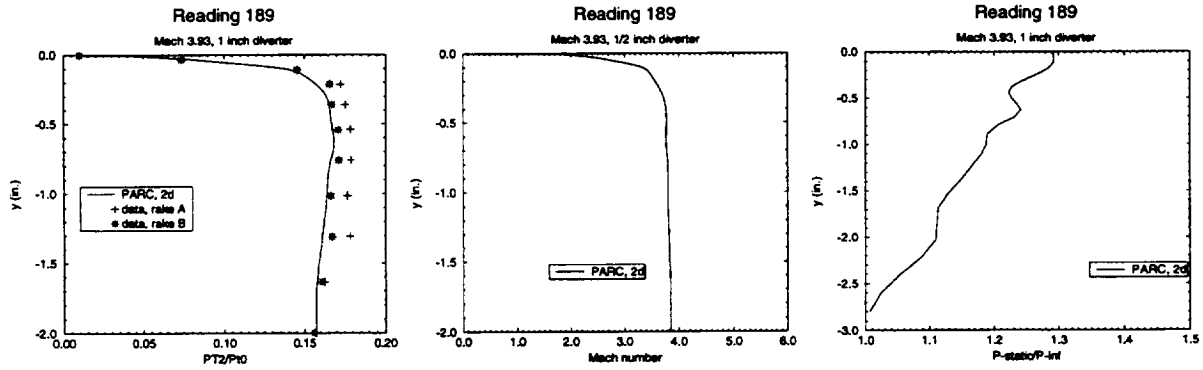

Figure 22: Boundary layer profiles for Mach 3.93 with 1.0 inch diverter height.

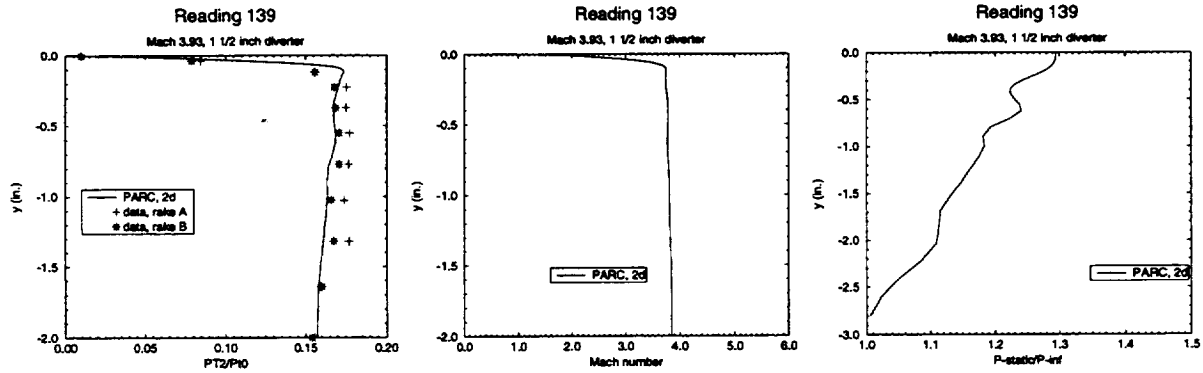

Figure 23: Boundary layer profiles for Mach 3.93 with 1.5 inch diverter height.

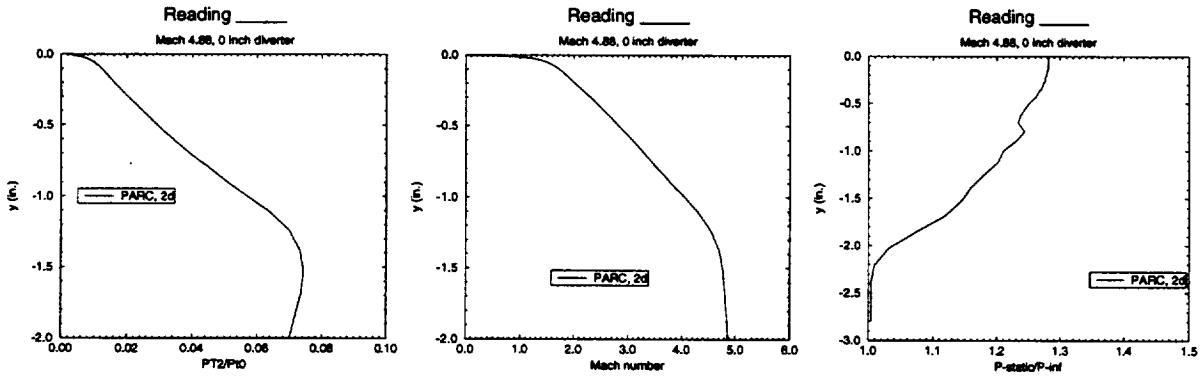

Figure 24: Boundary layer profiles for Mach 4.88 with 0.0 inch diverter height.

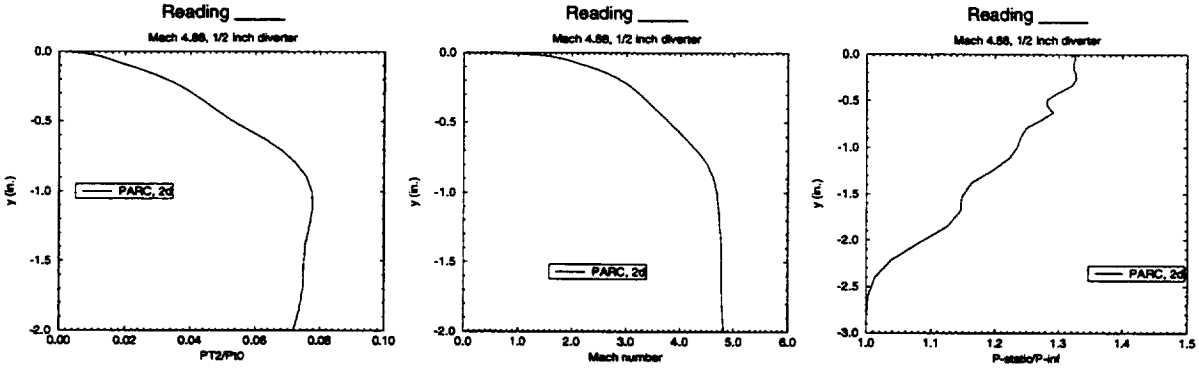

Figure 25: Boundary layer profiles for Mach 4.88 with 0.5 inch diverter height.

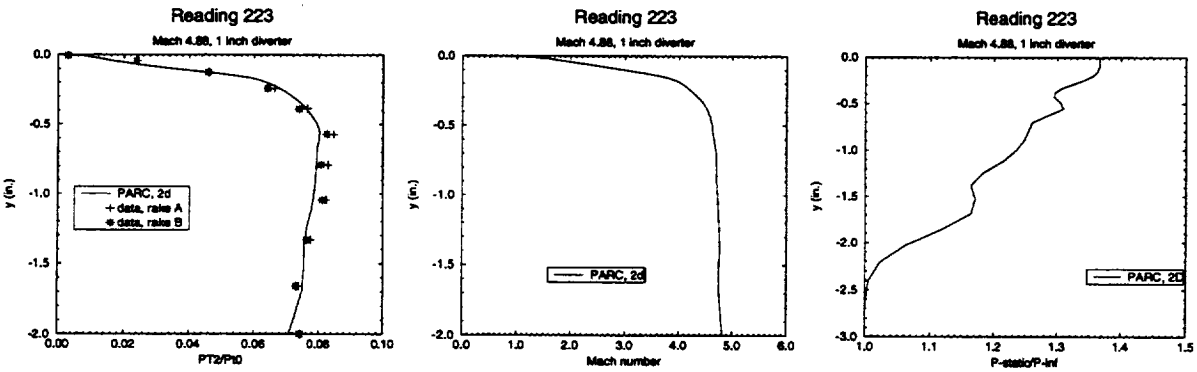

Figure 26: Boundary layer profiles for Mach 4.88 with 1.0 inch diverter height.

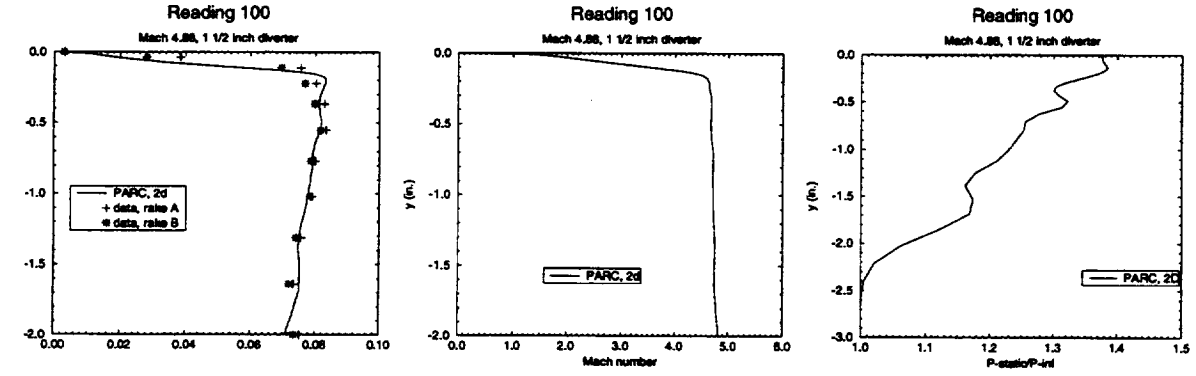

Figure 27: Boundary layer profiles for Mach 4.88 with 1.5 inch diverter height.

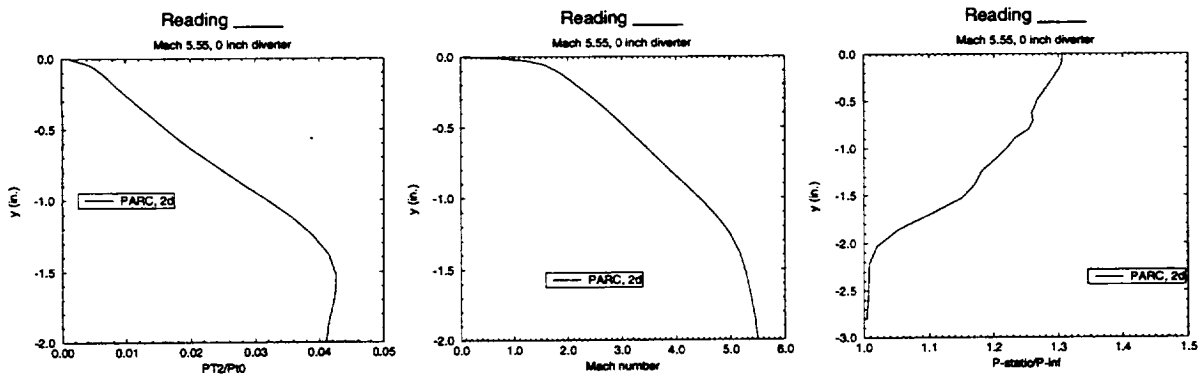

Figure 28: Boundary layer profiles for Mach 5.55 with 0.0 inch diverter height.

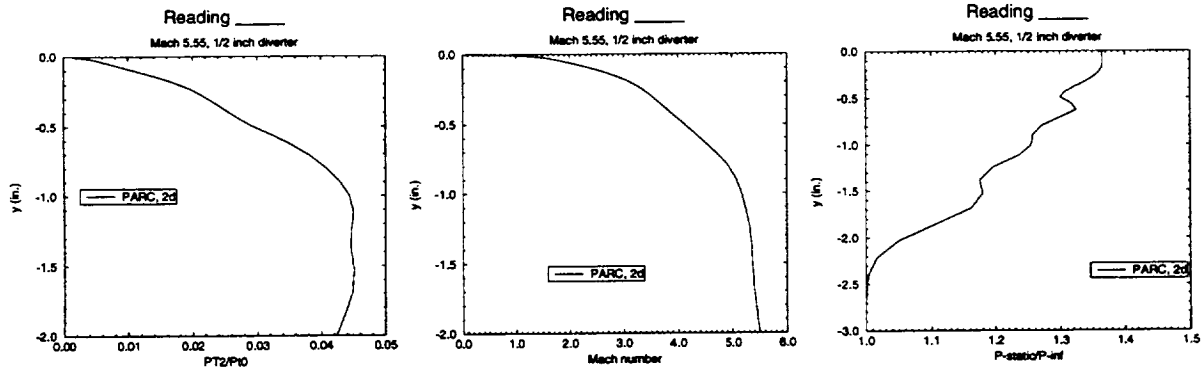

Figure 29: Boundary layer profiles for Mach 5.55 with 0.5 inch diverter height.

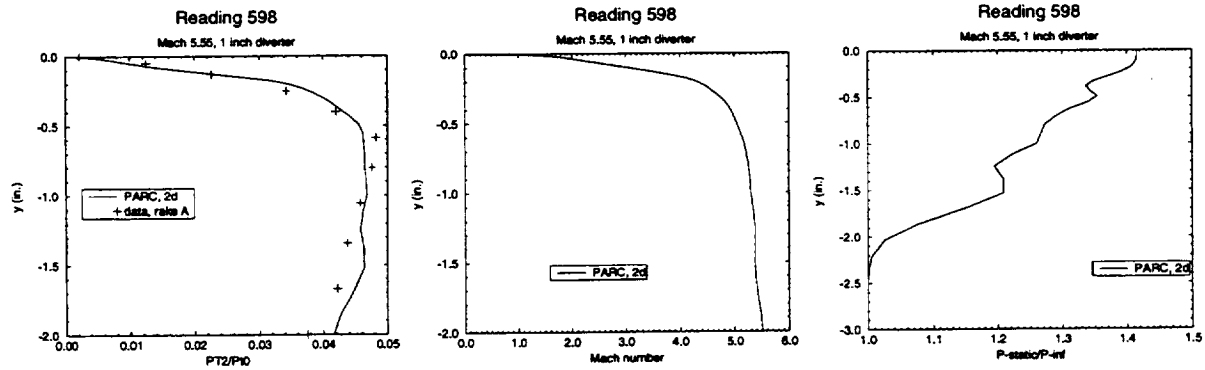

Figure 30: Boundary layer profiles for Mach 5.55 with 1.0 inch diverter height.

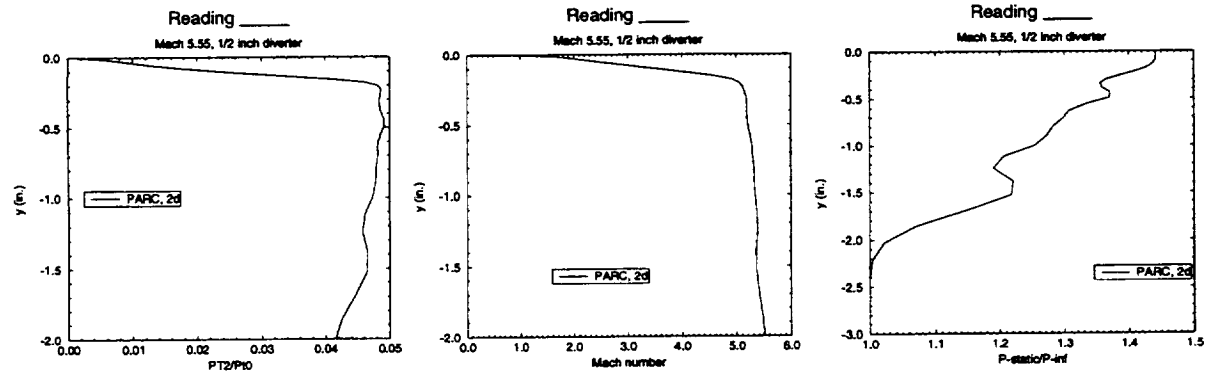

Figure 31: Boundary layer profiles for Mach 5.55 with 1.5 inch diverter height.

4 Mass Averaged Mach Numbers Across the Inlet Face

4.1 Objective

The objective of this study was to examine the effect that the diverter height and the cowl height had on the ingestion characteristics of the SSTO model. This was accomplished by calculating the mass averaged Mach numbers across the previously computed inlet cross sectional profiles.

4.2 Approach

The mass averaged Mach number was determined by integrating the computational solutions along the grid line which corresponds to the inlet face at x=11.3 inches. A simple trapezoidal integration technique was used for the following formula

$$\bar{M} = \frac{\int_{wall}^{cowll.e.} \rho \hat{U} M dy}{\int_{wall}^{cowll.e.} \rho \hat{U} dy} \tag{3}$$

where $\hat{U}$ was the velocity component parallel to the wall. The outer limits of integration were adjusted to simulate six different cowl heights varying from 0.5 inches to 3.0 inches.

The mass averaged Mach number distribution in relation to cowl and diverter heights is given in Table 7. These results are also plotted in Figure 32. The curves fits in this figure were obtained using a second degree least squares fit through the computed Mach numbers. As expected, as the diverter height increases or the cowl height increases the influence of the incoming facility boundary layer is diminished and all curves asymptotically approach the inviscid limit.

At Mach 2.90, a diverter height of one inch appears to place the model above the facility boundary layer edge as there is no difference between the curves at 1.0 and 1.5 inches. For this case, there is the smallest deviation in Mach number, approximately 35%, at the smallest cowl height when compared to the other flow conditions. For the other conditions, this deviation in mass averaged Mach number increases as the Reynolds number decreases owing to the greater influence of the facility boundary layer growth. At Mach 3.93 there is a 47% variation in the mass averaged Mach number depending on the diverter height. At Mach 5.55, this variation increases to 51% at the smallest cowl height. Figure 32 shows the mass averaged Mach number values which can be obtained by adjusting the cowl height for a specified boundary layer thickness.

4.3 Conclusions

The mass averaged Mach number at the inlet cross sectional face was seen to be sensitive to both the diverter height and the cowl height. As either of these were increased, the mass averaged Mach number asymptotically approached the inviscid limit as the influence of the boundary layer thickness became weaker.

References

[1] G.K. Cooper and J.R. Sirbaugh. PARC code: Theory and usage. AEDC TR-89-15, December 1989.

[2] E.W. Jr. Dorrel and M.D. McClure. 3D INGRID: Interactive three-dimensional grid generation. AEDC TR-87-40, April 1988.

[3] Charles J. Trefny and Jeanne C. De Bonis. Results of a single-expansion-ramp nozzle experiment with hot exhaust and external burning. NASA TM-106390, 1994.

cowl height inches	Mach no.	diverter height 0.00 in.	diverter height 0.50 in.	diverter height 1.00 in.	diverter height 1.50 in.
0.5	2.90	1.7639	2.3500	2.6253	2.6380
1.0	2.90	2.1563	2.5681	2.7004	2.7083
1.5	2.90	2.4574	2.6686	2.7415	2.7462
2.0	2.90	2.5531	2.7054	2.7596	2.7631
2.5	2.90	2.5983	2.7244	2.7704	2.7734
3.0	2.90	2.6504	2.7476	2.7842	2.7866
0.5	3.93	1.9763	2.8500	3.5203	3.6620
1.0	3.93	2.6065	3.3002	3.6439	3.7135
1.5	3.93	3.2561	3.5507	3.7165	3.7557
2.0	3.93	3.4186	3.6240	3.7484	3.7778
2.5	3.93	3.4853	3.6567	3.7643	3.7902
3.0	3.93	3.5879	3.7108	3.7945	3.8150
0.5	4.88	2.2495	3.1443	4.0889	4.3619
1.0	4.88	3.0346	3.8899	4.3923	4.5171
1.5	4.88	4.0537	4.3624	4.5638	4.6188
2.0	4.88	4.2748	4.4677	4.6125	4.6544
2.5	4.88	4.3474	4.5146	4.6461	4.6839
3.0	4.88	4.4839	4.6006	4.6985	4.7272
0.5	5.55	2.4414	3.4131	4.4156	4.7929
1.0	5.55	3.3304	4.2529	4.8276	5.0275
1.5	5.55	4.5266	4.8953	5.1056	5.1923
2.0	5.55	4.8181	5.0297	5.1926	5.2601
2.5	5.55	4.9021	5.0840	5.2306	5.2915
3.0	5.55	5.0780	5.1990	5.3037	5.3489

Table 10: Mass averaged Mach numbers at various cowl and diverter heights.

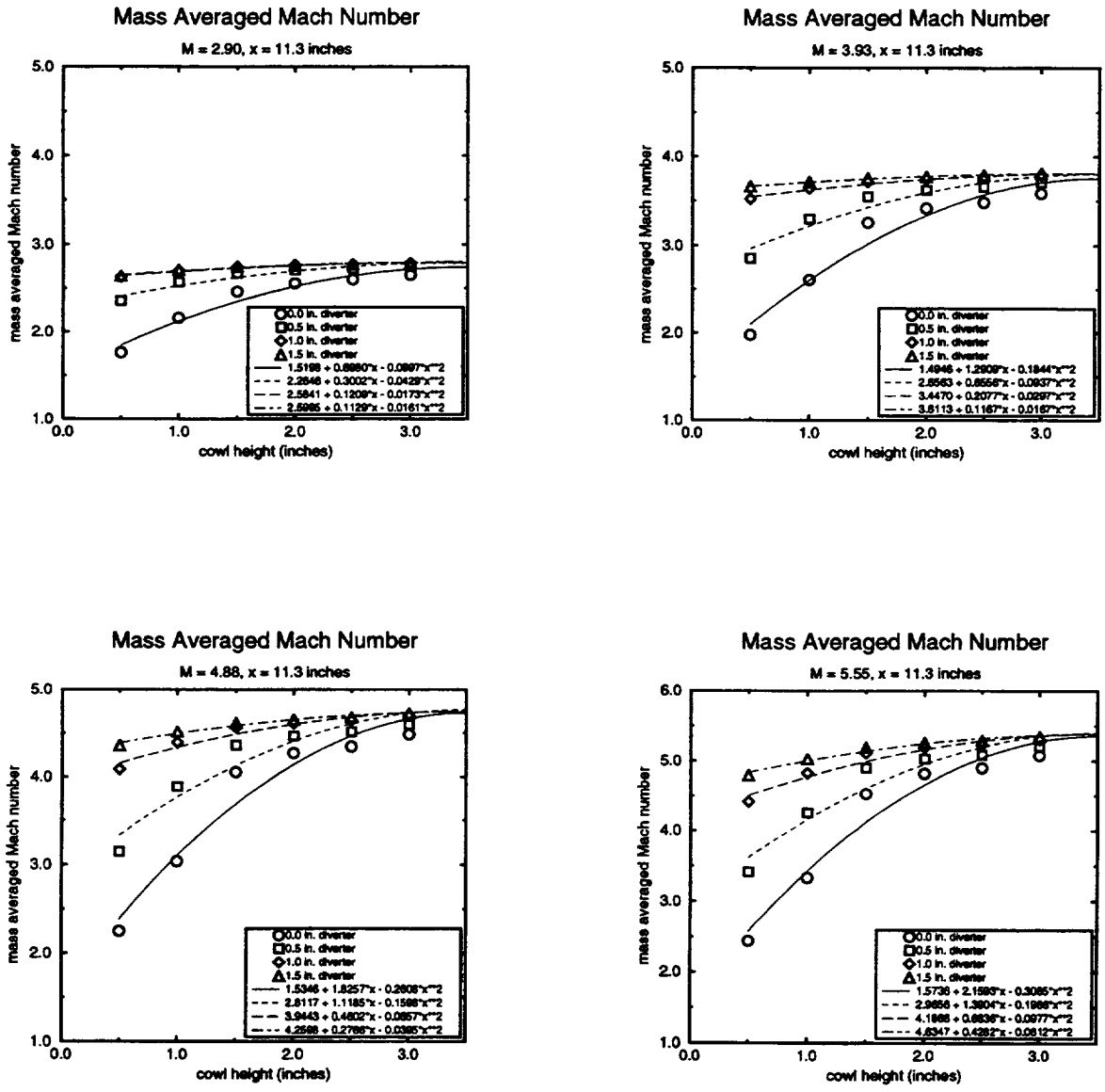

Figure 32: Mass averaged Mach numbers across the inlet profile at $x = 11.3$ for various cowl heights.

REPORT DOCUMENTATION PAGE

Form Approved
OMB No. 0704-0188

1. AGENCY USE ONLY (*Leave blank*)	2. REPORT DATE	3. REPORT TYPE AND DATES COVERED
	October 1994	Technical Memorandum

4. TITLE AND SUBTITLE

Computational Analysis in Support of the SSTO Flowpath Test

5. FUNDING NUMBERS

WU-505-70-59

6. AUTHOR(S)

Beverly S. Duncan and Charles J. Trefny

7. PERFORMING ORGANIZATION NAME(S) AND ADDRESS(ES)

National Aeronautics and Space Administration
Lewis Research Center
Cleveland, Ohio 44135-3191

8. PERFORMING ORGANIZATION REPORT NUMBER

E-9179

9. SPONSORING/MONITORING AGENCY NAME(S) AND ADDRESS(ES)

National Aeronautics and Space Administration
Washington, D.C. 20546-0001

10. SPONSORING/MONITORING AGENCY REPORT NUMBER

NASA TM-106757

11. SUPPLEMENTARY NOTES

Beverly S. Duncan, NYMA, Inc., Engineering Services Division, 2001 Aerospace Parkway, Brook Park, Ohio 44142 (work funded by NASA Contract NAS3-27186), and Charles J. Trefny, NASA Lewis Research Center. Responsible person, Charles J. Trefney, organization code 2701, (216) 433-2162.

12a. DISTRIBUTION/AVAILABILITY STATEMENT

Unclassified - Unlimited
Subject Category 34

12b. DISTRIBUTION CODE

13. ABSTRACT (*Maximum 200 words*)

A synergistic approach of combining computational methods and experimental measurements is used in the analysis of a hypersonic inlet. There are four major focal points within this study which examine the boundary layer growth on a compression ramp upstream of the cowl lip of a scramjet inlet. Initially, the boundary layer growth on the NASP Concept Demonstrator Engine (CDE) is examined. The follow-up study determines the optimum diverter height required by the SSTO Flowpath test to best duplicate the CDE results. These flow field computations are then compared to the experimental measurements and the mass average Mach number is determined for this inlet.

14. SUBJECT TERMS

Boundary layer flow; Inlet fluid dynamics

15. NUMBER OF PAGES

24

16. PRICE CODE

A03

17. SECURITY CLASSIFICATION OF REPORT	18. SECURITY CLASSIFICATION OF THIS PAGE	19. SECURITY CLASSIFICATION OF ABSTRACT	20. LIMITATION OF ABSTRACT
Unclassified	Unclassified	Unclassified	